IOP Publishing Nanotechnology
Nanotechnology 26 (2015) 295702 (6pp) doi:10.1088/0957-4484/26/29/295702

Raman shift and electrical properties of MoS_2 bilayer on boron nitride substrate

Lijun Li[1], Inyeal Lee[1], Dongsuk Lim[1], Moonshik Kang[1,2], Gil-Ho Kim[1], Nobuyuki Aoki[3], Yuichi Ochiai[3], Kenji Watanabe[4] and Takashi Taniguchi[4]

[1] School of Electronic and Electrical Engineering and Sungkyunkwan University Advanced Institute of Nanotechnology, Sungkyunkwan University, Suwon 440-746, Korea
[2] Manufacturing Engineering Team, Memory Division, Samsung Electronics Co., Hwasung 445-701, Korea
[3] Graduate School of Advanced Integration Science, Chiba University, 1-33 Yayoi-cho, Inage-ku, Chiba 263-8522, Japan
[4] Advanced Materials Laboratory, National Institute for Material Science, 1-1 Namiki, Tsukuba, 305-0044, Japan

E-mail: ghkim@skku.edu and n-aoki@faculty.chiba-u.jp

Received 20 April 2015, revised 20 May 2015
Accepted for publication 4 June 2015
Published 2 July 2015

Abstract

We have fabricated a bilayer molybdenum disulphide (MoS_2) transistor on boron nitride (BN) substrate and performed Raman spectroscopy and electrical measurements with this device. The characteristic Raman peaks show an upshift about 2.5 cm^{-1} with the layer lying on BN, and a narrower line width in comparison with those on a SiO_2 substrate. The device has a maximum drain current larger than 1 μA and a high current on/off ratio of greater than 10^8. In the temperature range of 100 K–293 K, the two terminal gate effect mobility and the carrier density do not change significantly with temperature. Results of the Raman and electrical measurements reveal that BN is a suitable substrate for atomic layer electrical devices.

Keywords: MoS_2, Raman shift, mobility, on/off ratio

(Some figures may appear in colour only in the online journal)

In recent years, the electrical properties of devices made by mono- and few-layer molybdenum disulphide (MoS_2) have attracted great interest [1, 2]. As a member of the transition metal dichalcogenides, MoS_2 thin layers possess several qualities that graphene cannot compete with. Graphene has a linear energy dispersion relation and does not have a band gap. This restricts it from being used to make electrical switching transistors. While spin–orbit coupling can be greatly induced in hydrogenated graphene [3], pristine graphene lacks this sought after effect in the application of spintronic devices. MoS_2 has a band gap that changes from its bulk indirect value of 1.3 eV to the monolayer direct gap of 1.8 eV [4]. For monolayer MoS_2, the effect of spin–orbit interactions in the valence band makes it a very promising material in spin- and valleytronic devices [5–9]. Bilayer MoS_2, with a larger valley degeneracy with respect to its monolayer example, is expected to have larger mobility. Because of the retained inversion symmetry in the bilayer MoS_2, it lacks the spin valley physics described in the monolayer. However, by applying an electric field [10, 11], twisting a lattice angle between the layers [12], or by applying a strain [13], the inter-layer interaction can be tuned, and the structural symmetry can be broken. Therefore the spin–orbit interaction can be recovered in bilayer MoS_2, and be utilized in spin- and valleytronic devices.

The quality of the electrical behavior made by an exfoliated 2D layer is closely related to the substrate that it lies on. The impurity and defect trapped between the MoS_2 and the substrate have a negative effect on the performance of the devices. In the case of graphene, the mobility is highly enhanced when boron nitride (BN) is used instead of a SiO_2 substrate [14]. In order to improve performance, researchers have applied various substrates, e.g., aluminium oxide (Al_2O_3) [2], PMMA (polymethyl methacrylate) [15], high-k dielectric material [16] and BN [17, 18] for MoS_2. In BN

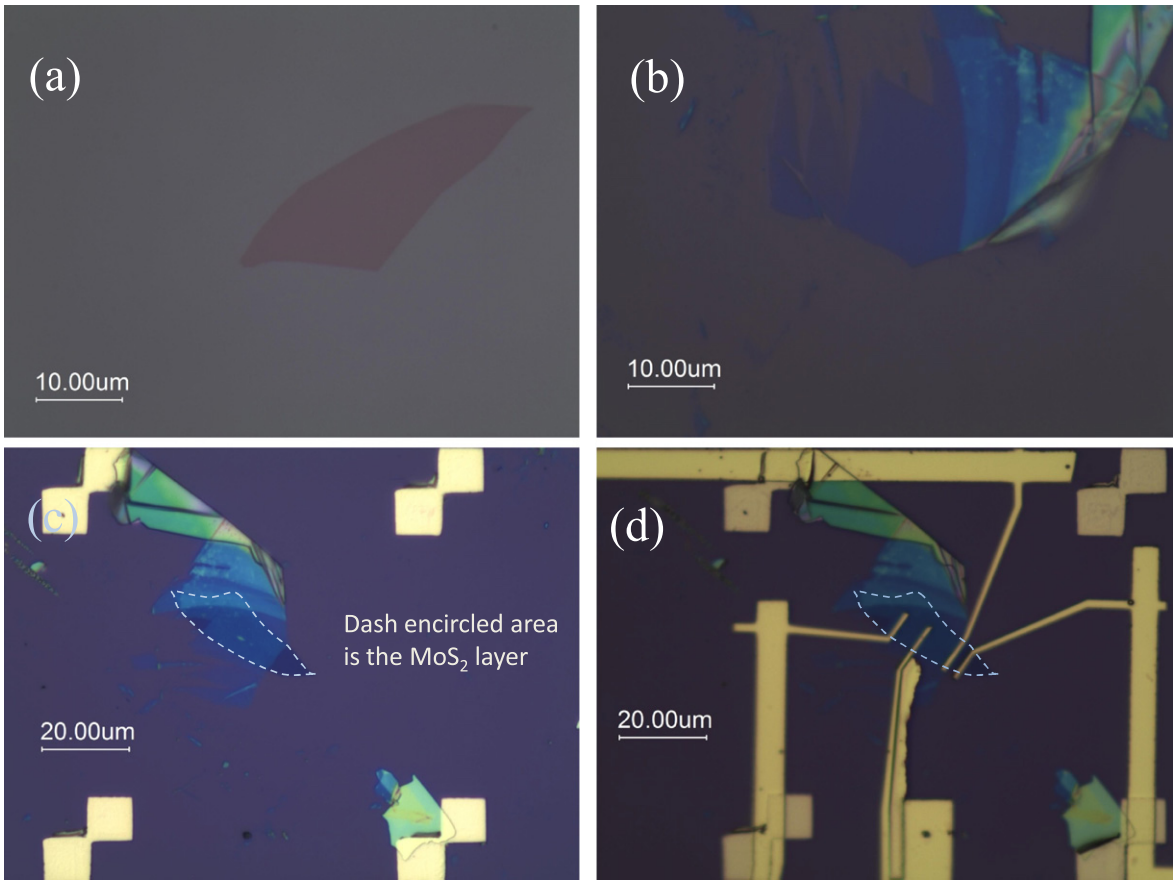

Figure 1. Optical image of the bilayer MoS_2 flake and the device. (a) Exfoliated MoS_2 layer on PMMA. (b) Exfoliated BN layer on SiO_2. (c) The MoS_2 layer transferred onto the BN layer. (d) The final device after e-beam patterning and metal evaporation.

encapsulated mono- and few-layer MoS_2, the mobility is greatly improved and quantum Hall effect was observed [19].

In this work we fabricated a bilayer MoS_2 transistor on BN substrate, and carried out Raman spectroscopy and electrical measurements. The characteristic Raman peaks exhibit an upshift with narrowed line width compared with those on SiO_2. The device has a high on/off ratio exceeding 10^8. The two terminal gate effect mobility, around 5–10 $cm^2\ V^{-1}\ s^{-1}$, does not show an obvious temperature dependence in the temperature range of 100–300 K.

The MoS_2 boron nitride heterostructure was made following the techniques of [14]. The MoS_2 layer was exfoliated by tape method from commercial crystal (purchased from SPI Supplies). The layer was deposited on a PMMA/PVA(polyvinyl alcohol) spin coated film supported by a silicon wafer (figure 1(a)). After the target MoS_2 layer was located, the Si wafer was floated on water to dissolve the PVA. The MoS_2 supported by the PMMA was picked up with a slide and transferred onto an exfoliated BN layer on a SiO_2/Si substrate (figures 1(b) and (c)). The SiO_2 layer has a thickness of 285 nm and the Si is highly doped to act as a back gate. After the transfer of MoS_2, the sample was annealed for two hours at 350 °C in flowing Ar/H_2 (1000/100 sccm) to clean the polymer residue [14]. Electrodes were patterned with e-beam lithography followed by metal Ti/Au(8/80 nm) deposition in an e-beam evaporation chamber with a base pressure of 3×10^{-6} Torr. After the device was made, another annealing at 350 °C in Ar/H_2 (1000/100 sccm) was carried out to reduce the contact resistance. The pressure of the annealing chamber remained at 4.6 Torr during the annealing. The device is shown in figure 1(d).

The Raman spectra [20], taken at ambient conditions, were presented in figure 2(d). The Raman signal at 524.5 cm^{-1} comes from the SiO_2 substrate. The frequency difference of the two characteristic vibration modes (E^1_{2g} and A_{1g}) of the MoS_2 layer is 22.1 cm^{-1} on the BN substrate, and 21.1 cm^{-1} on SiO_2. The optical contrast of the MoS_2 lying on PMMA is homogeneous, which means that it is unlikely that the layer has different thickness in different regions. Since the Raman spectra were taken after the annealing, it is natural to question whether the annealing could cause the layer to be oxidized and thinned unevenly. To clarify this doubt, we have checked the Raman shift peaks of MoO_3, MoO_2, and Mo_4O_{11} [21, 22] in the Raman spectra, but we have not found the relevant Raman peaks of these oxides. We consider that the difference in the Raman shift results from the MoS_2 and substrate interactions. The flake is confirmed to be a bilayer [20]. Increased peak separation of about 1 cm^{-1} on BN substrate for bilayer MoS_2 was reported in [23].

Compared to the layer on SiO_2, we observed that the E^1_{2g} and A_{1g} peaks of the layer on BN upshifted by 2.1 and

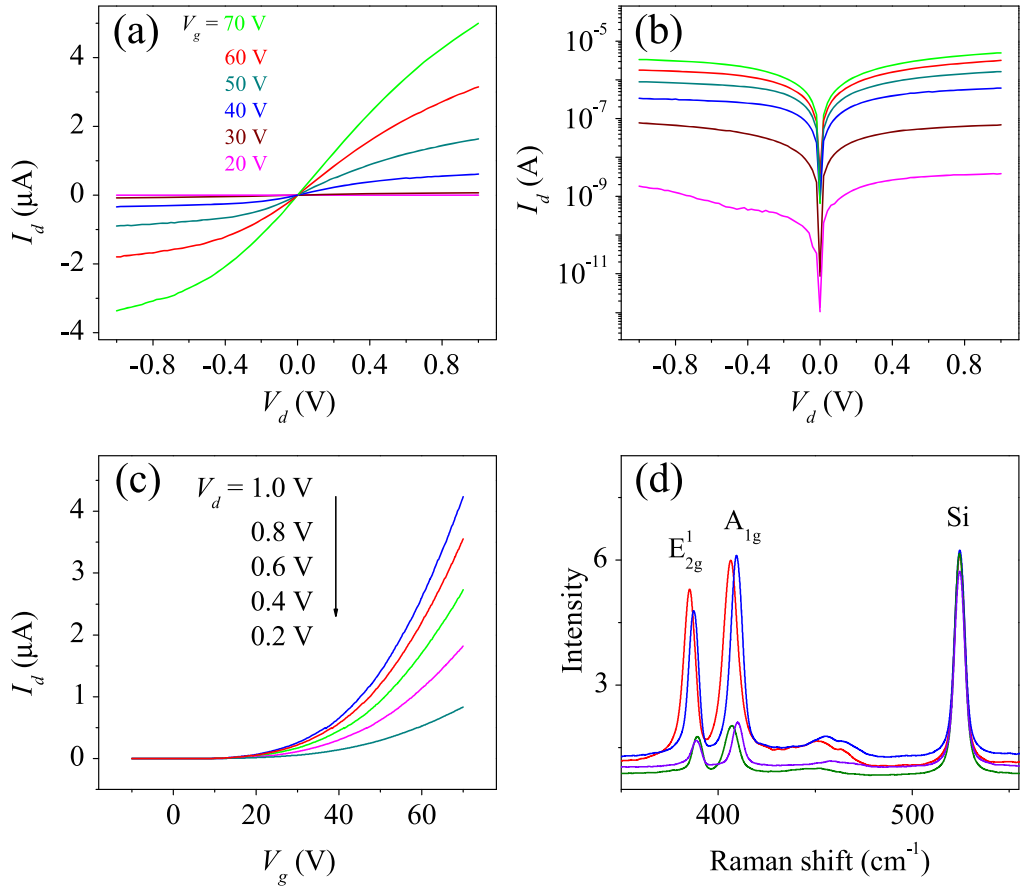

Figure 2. (a), (b) I_d as a function of V_d at various gate voltages V_g on linear and logarithmic scales. Measurements were taken at room temperature. (c) I_d as a function of V_g at various V_d. (d) The Raman spectra of the MoS_2 layers. Blue and red curves are Raman data of the fabricated device with the bilayer MoS_2 on BN and on SiO_2. Violet and green curves are Raman data from a monolayer sample on BN and on SiO_2.

Table 1. Comparison of the Raman spectra of the MoS_2 layers on a BN and SiO_2 substrate. △ represents the separation between the E^1_{2g} and A_{1g}. The unit is cm^{-1}.

	E^1_{2g}	A_{1g}	△	FWHM E^1_{2g}	FWHM A_{1g}
Bilayer on BN	387.4	409.5	22.1	5.8	7.3
Bilayer on SiO_2	385.3	406.5	21.2	7.1	8.6
Monolayer on BN	388.7	410.0	21.3	5.2	6.0
Monolayer on SiO_2	389.2	407.0	17.8	5.5	7.4

2.9 cm^{-1}, respectively; the line widths, calculated by the full widths at half maximum (FWHM), are narrower than those on SiO_2 (see the data presented in table 1). As a naive way of thinking, for the layer deposited on BN, with the super flatness of the exfoliated BN [24] and the similar lattice structure, the MoS_2 thin layer feels stronger inter-layer van der Waals interactions which leads to the stiffening (upshift) of the peaks, similar to the effect observed on A_{1g} when the layer number increases [20]. Physically, this can be explained by the screening effect from the dielectric substrate, which reduces the electron–phonon coupling and results in an upshift of the Raman peaks. For SiO_2 and BN, despite having roughly the same dielectric constant, the coupling between MoS_2 and exfoliated BN is stronger with respect to that between MoS_2 and SiO_2.

Carrier doping to the MoS_2 layer had been observed to result in the downshift of both A_{1g} and E^1_{2g} signals and increased line width, with less effect on E^1_{2g} [25]. In our sample, because the BN substrate has much fewer charged impurities and defects, i.e., the doping effect is less significant compared with that on SiO_2, the observed Raman signals show upshift and narrower line width. The upshift of frequency and line width narrowing of the graphene 2D peak on BN substrate has been reported in [26]. The reduced FWHM on BN is likely caused by the reduced substrate surface roughness and impurities.

We have also measured the Raman signals of a monolayer MoS_2 partly on BN and partly on SiO_2 substrate made by the same transfer method (see the violet and green curves in figure 2(d) and data presented in table 1). Interestingly we found that for monolayer MoS_2, the A_{1g} has a blue shift, but E^1_{2g} has a slight red shift when the substrate changes from SiO_2 to BN; the frequency difference changes from 17.8 cm^{-1} to 21.3 cm^{-1}. On the same substrate, A_{1g} peak position changes very slightly for mono- and bilayer (0.5 cm^{-1} on BN and on SiO_2), but E^1_{2g} has a pronounced red shift, which is 3.9 cm^{-1} on SiO_2 and 1.3 cm^{-1} on BN. It is worth noting that, on BN substrate, the frequency differences between E^1_{2g} and A_{1g} for mono- (21.3 cm^{-1}) and bilayer (22.1 cm^{-1}) are very close. Care should be taken when using Raman spectra to determine the layer number on BN.

The red shift of the E^1_{2g} when layer number increases from mono- to multilayers was explained by the enhancement of the dielectric screening of the long range Coulomb interactions between the effective charges [27]. In the experimental paper [23], the bilayer A_{1g} has an upshift of about 1 cm^{-1}, but E^1_{2g} stays unchanged as the substrate changes from SiO_2 to BN. In our bilayer sample both A_{1g} and E^1_{2g} have blue shifts >2 cm^{-1}. While the origin of the Raman spectra of atomic MoS_2 layers deserves further experimental and theoretical explorations, the observed results show that exfoliated BN can serve as a good substrate for MoS_2 with reduced electron–phonon coupling, which would effect a higher mobility in its electrical property.

The electrical measurements were performed with the semiconductor characterization system keithley 4200. The data in figure 2 were measured in ambient conditions. The source drain current and voltage curve, I_d versus V_d, is linear when V_d is smaller than 0.2 V. At gate voltages smaller than 20 V, the device has negligible conduction. The symmetric feature in figure 2(b) where I_d is on a logarithmic scale shows good performance of the device. Figure 1(c) shows the gate effect at various V_d.

After the room temperature experiments, the sample was coated with PMMA and kept in a vacuum sealed plastic bag. The device was kept in this state for 5 days until the low temperature measurements could be taken. When performing the low temperature experiments, the PMMA layer was kept intact except with an e-beam lithography to have the contact pads exposed. The results are shown in figure 3. Compared with the first measurement, this set of data shows lower threshold gate voltage. This is understandable, since the device is somewhat contaminated by some kind of air molecules with time elapsing, even though it had been kept in sealed plastic bag and was coated with PMMA. In spite of the contamination, the device shows a very high on/off ratio that exceeds 10^8. We attribute this to the effect of reduced impurity charge and crystal defect located in the BN/MoS_2 interface. We have not noticed an on/off ratio as high as this except for those with dual gated dielectrics by [1] on a monolayer and by [28] on a 15 nm thick layer.

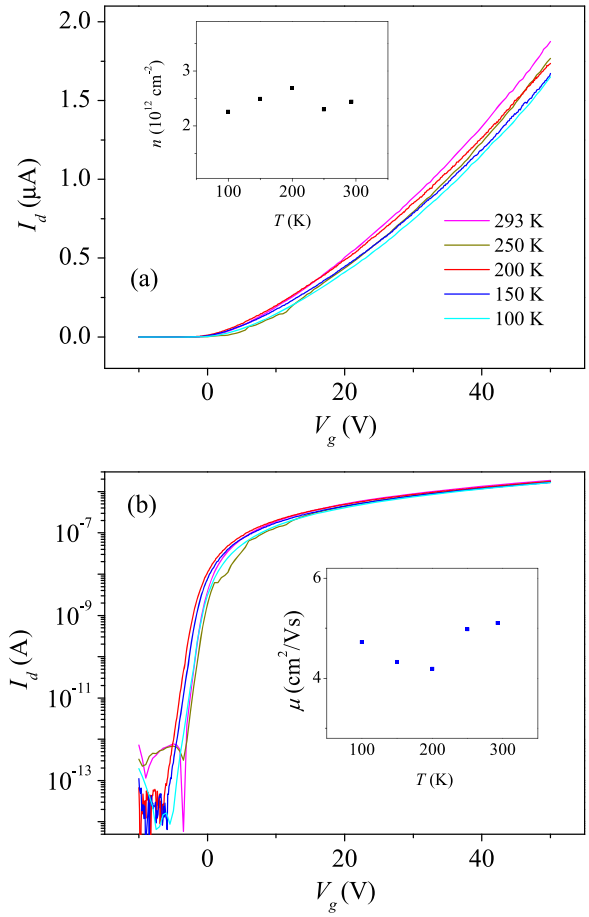

Figure 3. (a), (b) I_d as a function of V_g on linear and logarithmic scales at $T = 100$ K, 150 K, 200 K, 250 K, 293 K. $V_d = 0.6$ V. The inset in (a) is a plot of the variation of electron density n with temperature T. The inset in (b) presents the mobility μ extracted by expression (1) as described in main text.

The two terminal gate effect mobility was calculated from expression

$$\mu = \frac{dI_d}{dV_g} \cdot \frac{L}{WC_i V_d} \quad (1)$$

In (1), L and W are the length and width between source and drain electrodes. C_i is the capacitance per unit area between the back gate and the MoS_2 layer. Here, the BN layer thickness from our experience of optical contrast is around 5–10 nm. The dielectric constant of BN is $\varepsilon_1 = 4.0$ and that of the SiO_2 $\varepsilon_2 = 3.9$. We calculated the value $C_i = \frac{\varepsilon_0 \varepsilon_1 \varepsilon_2}{\varepsilon_2 d_1 + \varepsilon_1 d_2} = 11.7 \times 10^{-9}$ F cm^{-2}. $d_1 = 10$ nm, $d_2 = 285$ nm are the BN and SiO_2 layer thicknesses. The mobility extracted in this way is a rough estimate. Firstly, the two terminal mobility without knowing the contact resistance cannot describe the real channel mobility accurately, since the contact resistance is often comparable to or even larger than the channel resistance. Secondly, The total MoS_2 layer capacitance comprises a classical geometric part in series with a quantum capacitance that is not a constant value when electron density changes. At high electron density, the

charging capacitance closely approaches the classic geometric capacitance, but at low densities particularly close to pinch off, the quantum capacitance plays an importance role.

With this in mind, we only calculated the mobility at the largest gate voltage region to see qualitatively the temperature dependence. The results are presented in the inset of figure 3(b). μ varies in the range of 4.2–5.1 cm^2 V^{-1} s^{-1}. When the temperature is lowered μ shows an initial small decrease then a slight increase. This small change may come from the combined effects of a few aspects. Whilst the phonon limited true mobility increases with decreasing temperature, the contact resistance may increase with decreasing temperature and cover up the real change of the mobility; the degassing of the PMMA layer may also contribute to the measured mobility. The low temperature environment has a high vacuum (better than 10^{-6} Torr). Suppose that the air impurities trapped underneath the PMMA diffuses out with pumping, the mobility will increase with time until an equilibrium sets in. The mobility calculated from the room temperature measurement before coating PMMA is 9.3 cm^2 V^{-1} s^{-1}, which is almost double the value calculated from this set of data. This shows that the device has undergone a degradation with time by contamination.

We take a look at the MoS_2 layer mobilities observed from previous work. For monolayer MoS_2 it has been reported theoretically and experimentally that the mobilities follow an $\propto T^{-1.7}$ dependence [29, 30]. The Hall mobility of bilayer MoS_2 at the highly on state increases with $\propto T^{-1.1}$ [30] as the temperature is varied from 300 to 100 K. The bilayer mobility from [19] shows a $T^{-2.5}$ dependence. A recent calculation considering temperature dependent screened impurity scattering and the interaction with optical phonon modes in the dielectric environment shows that the monolayer MoS_2 mobility is limited by charged impurities at high impurity density, whilst the optical phonon scattering from the dielectrics determines the highest mobility [31] as the impurity density decreases. Although the phonon limited mobility at room temperature is predicted to be as high as 400 cm^2 V^{-1} s^{-1} [29], up to now no experimental result reaches this value.

From (1), and the 2D conductivity expression,

$$\sigma = \frac{I_d}{V_d}\frac{L}{W} = en\mu \tag{2}$$

the 2D electron density n can be expressed as

$$n = \frac{I_d C_i}{e}\frac{1}{\frac{dI_d}{dV_g}} \tag{3}$$

Here e is the electron charge. At the largest gate voltage the density does not show an obvious temperature dependence (see the inset in figure 3(a)). The average value of the density is $\sim 2.43 \times 10^{12}$ cm^{-2}. In the highly on state, the gate induced charge carriers far outnumber the charge carriers from background donors. The gate induced density depends solely on the gate voltage irrespective of the temperature.

In conclusion, we fabricated a bilayer MoS_2 device on a BN substrate. Raman spectra of the layers show that the characteristic peaks exhibit an upshift about 2.5 cm^{-1}, with sharper line widths compared to those on a SiO_2 substrate. The Raman data indicate a reduced electron–phonon interaction of MoS_2 on BN. Electrical measurements of this device at room and low temperatures show a current on/off ratio of greater than 10^8. The two terminal gate effect mobility, which does not show obvious temperature dependence in the measured temperature range, is limited by the contact resistance. The results reveal that boron nitride can serve as a suitable substrate for high performance atomic thin layer MoS_2 devices. In the future we expect to make electrodes with low contact resistance, and perform four terminal measurement to study the MoS_2 thin layer electrical properties in detail.

Acknowledgments

This paper was supported by Samsung Research Fund, Sungkyunkwan University, 2013. The authors are thankful to Shen Lai for the help in low temperature probe station measurement, and to Jaeho Jeon for measuring the Raman spectra.

References

[1] Radisavljevic B, Radenovic A, Brivio J, Giacometti J V and Kis A 2011 *Nat. Nanotechnology* **6** 147
[2] Kim A *et al* 2012 *Nat. Commun.* **3** 1011
[3] Balakrishnan J, Koon G K W, Jaiswal M, Castro Neto A H and zyilmaz B 2013 *Nat. Phys.* **9** 284
[4] Cheiwchanchamnangij T and Lambrecht W R L 2012 *Phy. Rev.* B **85** 205302
Mak K F, Lee C, Hone J, Shan J and Heinz T F 2010 *Phys. Rev. Lett.* **105** 136805
[5] Yuan H *et al* 2013 *Nat. Phys.* **9** 563
[6] Xiao D, Liu G, Feng W, Xu X and Yao W 2012 *Phys. Rev. Lett.* **108** 196802
[7] Zeng H, Dai J, Yao W, Xiao D and Cui X 2012 *Nat. Nanotechnology* **7** 490
[8] Jiang T, Liu H, Huang D, Zhang S, Li Y, Gong X, Shen Y, Liu W and Wu S 2014 *Nat. Nanotechnology* **9** 825
[9] Mak K F, McGill K L, Park J and McEuen P L 2014 *Science* **344** 1489
[10] Ramasubramaniam A, Naveh D and Towe E 2012 *Phys. Rev.* B **84** 205325
Liu Q, Li L, Li Y, Gao Z, Chen Z and Lu J 2012 *J. Phys. Chem.* C **116** 21556
[11] Wu S *et al* 2013 *Nat. Phys.* **9** 149
[12] Jiang T, Liu H, Huang D, Zhang S, Li Y, Gong X, Shen Y, Liu W and Wu S 2014 *Nat. Nanotechnology* **9** 825
[13] Koskinen P, Fampiou I and Ramasubramaniam A 2014 *Phys. Rev. Lett.* **112** 186802
[14] Dean C R *et al* 2010 *Nat. Nanotechnology* **5** 722
[15] Bao W, Cai X, Kim D, Sridhara K and Fuhrer M S 2013 *Appl. Phys. Lett.* **102** 042104
[16] Zhou C, Wang X, Raju S, Lin Z, Villaroman D, Huang B, Chan H L-W, Chanb M and Chai Y 2015 *Nanoscale* **7** 8695
[17] Chan M Y *et al* 2013 *Nanoscale* **5** 9572
[18] Lee G *et al* 2013 *ACS Nano* **9** 7931
[19] Cui X *et al* 2014 arXiv:1412.5977

[20] Lee C, Yan H, Brus L E, Heinz T F, Hone J and Ryu S 2010 *ACS Nano* **4** 2695
[21] Windom B C, Sawyer W G and Hahn D W 2011 *Tribol. Lett.* **42** 301
[22] Dieterle M and Mestl G 2002 *Phys. Chem. Chem. Phys.* **4** 822
[23] Buscema M, Steele G A, van der Zant H S J and Castellanos-Gomez A 2013 arXiv:1311.3869
[24] Xue J, Javier Sanchez-Yamagishi J, Bulmash D, Jacquod P, Deshpande A, Watanabe K, Taniguchi T, Jarillo-Herrero P and LeRoy B J 2011 *Nat. Mater.* **10** 282
Yankowitz M, Xue J and LeRoy B J 2014 *J. Phys.: Condens. Matter* **26** 303201
[25] Chakraborty B, Achintya Bera A, Muthu D V S, Bhowmick Somnath, Waghmare U V and Sood A K 2012 *Phys. Rev.* B **85** 161403(R)
[26] Wang L, Chen Z, Dean C R, Taniguchi T, Watanabe K, Brus L E and Hone J 2012 *ACS Nano* **6** 9314
[27] Molina-Sanchez A and Wirtz L 2011 *Phys. Rev.* B. **84** 155413
[28] Liu H and Ye P D 2012 *IEEE Electron Device Lett.* **33** 546
[29] Kaasbjerg K, Thygesen K S and Jacobsen K W 2012 *Phys. Rev.* B **85** 115317
[30] Baughter B W H, Churchill H O H, Yang Y and Jarillo-Herrero P 2013 *Nano Lett.* **13** 4212
[31] Ma N and Jena D 2014 *Phys. Rev.* X **4** 011043